Copy
RM L54G23a

NACA

RESEARCH MEMORANDUM

STABILITY AND DRAG CHARACTERISTICS AT MACH NUMBERS FROM 0.8 TO 1.5 OF A FREE-FLIGHT MODEL HAVING 3-PERCENT-THICK, 60° TRIANGULAR WING AND HORIZONTAL TAIL SURFACES

By Rowe Chapman, Jr., and Harvey A. Wallskog

Langley Aeronautical Laboratory
Langley Field, Va.

NATIONAL ADVISORY COMMITTEE
FOR AERONAUTICS

WASHINGTON

August 30, 1954

NATIONAL ADVISORY COMMITTEE FOR AERONAUTICS

RESEARCH MEMORANDUM

STABILITY AND DRAG CHARACTERISTICS AT MACH NUMBERS FROM 0.8 TO 1.5 OF A FREE-FLIGHT MODEL HAVING 3-PERCENT-THICK, 60° TRIANGULAR WING AND HORIZONTAL TAIL SURFACES

By Rowe Chapman, Jr., and Harvey A. Wallskog

SUMMARY

A flight test of a rocket-propelled model having 60° triangular wing and horizontal tail surfaces 3 percent thick was made and data were obtained on the drag and stability characteristics. Analysis of the data and comparison with other data on triangular-wing configurations indicated that no severe penalty in zero-lift drag was experienced because of the addition of a horizontal tail and a single vertical tail to a low drag configuration.

The trimmed drag for a lift coefficient of 0.125 at a Mach number of 1.4 is 57 percent greater than the zero-lift drag for that Mach number.

The forcing of longitudinal motions by lateral oscillations can be a factor in causing a portion of the low amplitude oscillations in the longitudinal plane.

INTRODUCTION

A rocket-propelled model having a 3-percent-thick, 60° triangular wing and a 60° triangular horizontal tail was flight tested to obtain the stability and drag under lifting conditions. The design of the model used in this investigation paralleled that of a general research vehicle, used for zero-lift drag investigations, on which low drag coefficients have been obtained (ref. 1). The primary external difference between the present model and the general research model was the presence of a single vertical tail and a horizontal tail; hence, the present model more nearly represented a possible low-drag airplane configuration.

A pulsing system for disturbing the model in pitch by movement of the horizontal tail at a preset frequency was incorporated for the purpose of obtaining the variation of drag with lift over the Mach

number range. Difficulty was experienced with the unconventional pulsing system. The final result during flight test was one long pulse after which the horizontal tail returned and remained at zero incidence. This equipment failure limited the data obtained from the flight test.

An analysis of the flight time history was made to obtain some of the basic aerodynamic coefficients that determine the performance and stability of the configuration. A portion of the flight time history evidenced coupled lateral and longitudinal motions; this motion is discussed in detail in regard to the frequencies present in the flight record.

The model was flown at the Langley Pilotless Aircraft Research Station at Wallops Island, Va.

SYMBOLS

C_N normal-force coefficient, $\frac{a_n}{g}\frac{w}{qS}$

C_C chord-force coefficient, $\frac{-a_l}{g}\frac{w}{qS}$

C_L lift coefficient, $C_N \cos \alpha - C_C \sin \alpha$

C_D drag coefficient, $C_C \cos \alpha + C_N \sin \alpha$

C_m pitching-moment coefficient

C_Y side-force coefficient, $\frac{a_t}{g}\frac{w}{qS}$

C_n yawing-moment coefficient

a_n normal acceleration as obtained from accelerometer, ft/sec^2

a_l longitudinal acceleration as obtained from accelerometer, ft/sec^2

a_t transverse acceleration as obtained from accelerometer, ft/sec^2

w model weight, lb

g acceleration of gravity, ft/sec^2

p	free-stream static pressure, lb/sq ft
p_o	standard sea-level static pressure, lb/sq ft
V	velocity, ft/sec
q	dynamic pressure, $\frac{1}{2}\gamma pM^2$, lb/sq ft
M	Mach number
γ	specific heat ratio (1.40)
S	wing area (including area within the fuselage), sq ft
R	Reynolds number, based on wing mean aerodynamic chord
$\bar{c}$	wing mean aerodynamic chord, ft
x	longitudinal distance along body axis from nose, in.
r_e	radius of equivalent body of revolution, in.
A	cross-sectional area in plane normal to body axis, $in.^2$
l	body length, in.
I_Y	moment of inertia about Y-axis, $slug\text{-}ft^2$
I_Z	moment of inertia about Z-axis, $slug\text{-}ft^2$
I_X	moment of inertia about X-axis, $slug\text{-}ft^2$
ϵ	inclination of principal axis to longitudinal axis of model, deg
α	angle of attack, deg
β	angle of sideslip, deg
η	angle of attack of principal longitudinal axis of inertia, $\eta = \alpha - \epsilon$, deg
θ	angle of pitch, radians
δ	incidence of horizontal tail, deg
P	period of oscillation, sec

t time, sec

$\dot{\alpha}$ rate of change of angle of attack, $\frac{1}{57.3}\frac{d\alpha}{dt}$, radians/sec

q rate of change of angle of pitch, $d\theta/dt$

$C_{m_q} = \frac{dC_m}{d\frac{q\bar{c}}{2V}}$

$C_{m_{\dot{\alpha}}} = \frac{dC_m}{d\frac{\dot{\alpha}\bar{c}}{2V}}$

$C_{n_\beta}{}^*$ static-directional-stability derivative as obtained from the formula $C_{n_\beta}{}^* = \frac{4\pi^2 I_Z}{qSbP^2}$

$T_{1/2}$ time to damp to one-half amplitude, sec

Subscripts:

T trimmed, or mean value

The symbols α and β used as subscripts indicate the derivative of the quantity with respect to the subscripts.

MODEL AND INSTRUMENTATION

Model Description

The general arrangement of the model is shown in figure 1(a), a three-view drawing of the model. Figure 1(b) is an area-distribution plot for the model, showing the geometric relationship between the model and its equivalent body of revolution. Photographs of the model are presented as figure 2. Pertinent geometric and mass characteristics of the model are given in table I.

Fuselage construction was of laminated wood with metal rings from station 25 to station 120.5 and housed an ABL Deacon sustainer rocket motor, the principal power plant. A spun metal nose and tail completed the fuselage. The space inside the nose cone was utilized to house the telemetry. Batteries, hydraulic accumulator, and accelerometers were

located in compartments routed into the wooden fuselage and accessible through metal hatches. The hydraulic actuator for the tail surface was located inside the hollow rear portion of the vertical tail.

The wing was of composite wood and metal construction, aluminum overlays, and trailing-edge inserts. The horizontal tail surface was geometrically similar to the wing and was machined of solid aluminum. The vertical tail was a constant thickness of 7/8 inch at the juncture of the straight trailing edge and the contoured forward portion.

The pulsing system for the horizontal tail was designed on the principle of an unbalanced force existing between a spring and the hydraulic fluid acting on a piston. Since no measurements pertaining to the operation of the pulsing system were telemetered, reasons for improper operation during flight could not be ascertained.

Instrumentation

The model contained a standard NACA eight-channel telemeter which transmitted continuous flight measurements of angle of attack, normal acceleration at the center of gravity, normal acceleration at the nose, transverse acceleration, longitudinal acceleration, horizontal tail position, free-stream total pressure, and a reference static pressure.

Model position in space was determined from an SCR 584 radar tracking unit and model velocity was obtained by use of a CW Doppler velocimeter unit. Atmospheric data were obtained from a radiosonde released just prior to model flight.

TEST AND ANALYSIS

Test

The model was launched at an elevation angle of approximately 60° utilizing a mobile launcher. Figure 2(b) is a photograph of the model on the launcher and shows the 5.0-inch high-performance air-to-ground (HPAG) rocket motor used for a booster. The booster propelled the combination to a Mach number of approximately 0.3 at which time the sustainer rocket motor fired, separating the model and booster. The model attained a maximum Mach number of 1.51 at sustainer burnout.

The velocity of the model from radar was corrected for the curved flight path and this in conjunction with the atmospheric data from the position radar plots was used to compute the Mach number. The static pressure from radiosonde data and radar position plots was used for all

data reduction. A check on the Mach number by use of the total pressure and static pressure was made and a maximum disagreement in Mach number of 0.03 was obtained from peak Mach number to a Mach number of 1.42. Data corrections were applied in accordance with the accepted procedures as are given in references 2 and 3.

Figure 3 gives the variation of the test conditions with Mach number for the power-off portions of the flight. In figure 3(a), the Reynolds number is based on the mean aerodynamic chord of the wing.

Analysis

The analyses are based on the assumption of constant coefficients in the differential equations of motion which in turn are for small disturbances from trim conditions.

Oscillations of the normal acceleration and angle of attack were analyzed by use of the method presented in reference 4. Oscillations of the lateral accelerometer were analyzed by the use of the formula presented in reference 5.

The periodic motion recorded by the normal accelerometer after the horizontal tail returned to the zero incidence position was not easily identified. A repetitive pattern on the accelerometer trace indicated that a steady-state type of motion was occurring. Since the lateral motion was of sinusoidal character, any forcing of the motion in the normal plane should also have sinsuoidal characteristics. A harmonic analysis of the normal accelerometer trace was made in order to separate and identify the frequencies present on the record. The numerical method, Runge's schedule, presented in reference 6 was used to accomplish the harmonic analysis.

Accuracy

The telemetered data are believed to be accurate to within ±1 percent of the full-scale range of the respective instruments. Converted to coefficient form, the probable errors in the basic coefficients and angle of attack are as follows:

M	ΔC_N	ΔC_C	$\Delta\alpha$, deg
0.8	0.023	0.002	0.15
1.5	.008	.0007	.15

A portion of the errors presented in the aforementioned table are introduced by possible errors in dynamic pressure. The error in dynamic pressure is estimated to be less than 0.28 lb/sq in. at subsonic speeds and less than 0.50 lb/sq in. at supersonic speeds. The possible error in Mach number is of the order of ±0.02. This error can in part explain the discrepancy in Mach number between that computed from total pressure and that obtained from radar.

RESULTS AND DISCUSSION

Performance

Figure 4 presents the variation of the horizontal tail incidence with Mach number. The solid line is for power-off flight and the broken line is for power-on flight; below $M = 1.06$ the tail incidence remained at zero for the power-on condition. Analysis of the data was made from various portions of the record where the model maneuvered.

Longitudinal trim.- Figure 5 shows the trim characteristics of the model. The solid lines are the C_L and α trim for the power-off portion of the flight. The broken line is the trim angle of attack for the power-on condition, and, at Mach numbers less than 1.1, it represents the trim attitude necessary to counteract the pitching moment caused by the rocket motor. The power-on curve is shown for the purpose of relating the attitude of the model to the lateral stability during the accelerating portions of the flight.

The changes in trim angle of attack for the power-off condition are a primary result of the changing incidence of the horizontal tail. The changes in trim lift coefficient as contrasted to the changes in trim angle-of-attack are additionally affected by a changing lift-curve slope. The transonic region was traversed with no abrupt changes in trim for the low angles of attack of this test.

Lift.- Figure 6 is a plot showing the variation of C_L and C_N with α during the two maneuvers caused by the moving horizontal tail. The Mach number and horizontal-tail position corresponding to the lift and angle of attack are shown in the figure.

Figure 7 is a plot of the slopes of the C_L against α curves as a function of Mach number. Additional points of C_{L_α} were obtained from low-range α variations at the subsonic Mach numbers and are also shown in figure 7.

For comparison a curve of C_{L_α} for an airplane configuration having a 60° triangular wing but no horizontal tail is shown in figure 7. This curve is from reference 7 and is for a model with a 6.5-percent-thick wing, $\delta = 0^\circ$ and power-off conditions. An additional comparison is provided by the curve labeled reference 8, which is for the wing plus wing-body interference. This curve is for configuration A from reference 8 and these data agree very well with the low-lift data from the present test. The supersonic C_{L_α} seems to agree in level with the data from reference 7; however, the transonic level is somewhat higher.

Drag.- Presented in figure 8 are the power-off drag coefficients plotted as a function of lift coefficient for $M = 1.32$. The lift coefficient and tail-incidence values correspond to those shown in figure 6(b) and additional points for $M = 1.49$ are included.

A single value of the induced drag parameter $dC_D/dC_L^2 = 0.51$ at $M = 1.32$ was calculated by utilizing the curve presented in figure 8. This value of induced drag corresponds to the trimmed value since the tail deflection δ was changing slowly. Untrimmed induced drag measurements were presented in reference 7 for a delta-wing configuration where the elevon controls were changed abruptly from $\delta = 0^\circ$ to $\delta = -9^\circ$ and in reference 9 for a delta-wing model which had an unswept horizontal tail that was pulsed abruptly from $\delta = -1.16^\circ$ to $\delta = -5.43^\circ$. From these data estimates of the trimmed dC_D/dC_L^2 were obtained.

The untrimmed value of dC_D/dC_L^2 for the tailless delta-wing model of reference 7 (6.5-percent-thick wing) varied from approximately 0.35 ($\delta = 0^\circ$) to 0.40 ($\delta = -9^\circ$) and the estimated trimmed value was about 0.6. For the delta-wing model with an unswept tail (ref. 9), the untrimmed dC_D/dC_L^2 varied from about 0.2 ($\delta = -1.16^\circ$) to 0.3 ($\delta = -5.43^\circ$) and the estimated trimmed value was approximately 0.4. Hence, it appears that, although the induced drag obtained from the present model was high, it compares favorably with other tests, since it is lower than the corresponding value estimated for a tailless model and higher than that obtained from a model which had an unswept tail that was relatively larger and placed farther rearward.

The maximum L/D obtained from the present test was 4.4 at a value of C_L of 0.12 compared with 7.0 reported in reference 1 for a model with the same wing-fuselage combination but with a different empennage. The low value of $(L/D)_{max}$ from the present test was a result of the high trimmed induced drag, whereas the reference data utilized untrimmed values of dC_D/dC_L^2.

Illustrated in figure 9 are the measured drag coefficients plotted against Mach number. Corresponding trim lift coefficients are shown in figure 5(a). The point on figure 9 labeled zero-lift drag was obtained by extrapolating the drag polar of figure 8 to $C_L = 0$. At Mach numbers below about 1.3 the measured drag data presented correspond very nearly to zero-lift drag. The dashed line in figure 9 labeled reference 1 is the zero-lift drag of the general research vehicle which was the same configuration as that of the present test except for the empennage. The solid line in figure 9 is the estimated zero-lift drag for the present test and was obtained by drawing the curve through the zero-lift drag point (from the drag polar) and parallel to the drag curve of the reference model. From figure 9 it is apparent that the zero-lift drag penalty caused by the change in the empennage was about 0.0020. Fin drag for the reference model was experimentally determined to be about 0.0012 at supersonic speeds. The increments in drag from the estimated zero-lift drag and the measured drag points are indicative of the drag due to lift for $\delta = -8^\circ$ of the present model. The trimmed drag and lift coefficients which resulted from a tail deflection of $\delta = -8^\circ$ at a Mach number of 1.4 were 0.0282 and 0.125, respectively. This drag increment corresponds to 57 percent increase in drag to obtain a lift coefficient of 0.125.

STABILITY

Longitudinal

Three primary motions occurred during the flight that provided data amenable to the linear analysis technique. When the sustainer motor fired, a transient oscillation was induced because of the pitching moment incurred from the thrust line not passing through the center of gravity of the model. From this oscillation the period of the model was measured and adjusted to the power-off inertia of the model. This period is plotted in figure 10 and is labeled power on. When the motion of the horizontal tail occurred, a transient oscillation followed and the period of this oscillation is plotted in figure 10 and is labeled as the power-off period.

Static.- The values of C_{m_α}, reduced from the period curve shown in figure 10, are plotted as a function of Mach number in figure 11. Data from reference 7 (for a tailless configuration having a different fuselage) are presented for comparison. These data from reference 7 for center-of-gravity locations of $0.20\bar{c}$ and $0.25\bar{c}$ bracket the curve obtained from the present test which is for a center-of-gravity location of $0.237\bar{c}$.

Dynamic.- Two data points of $C_{m_q} + C_{m_{\dot{\alpha}}}$ were obtained from analysis of the damping of the transient oscillation. These data points and a comparison with data from reference 7 are shown in figure 12. The comparison shown in figure 12 indicates that the horizontal tail was effective for increasing the damping of a triangular-wing configuration at $M = 1.3$.

Lateral

For the power-off condition and the trim attitude shown in figure 5, the model experienced dynamically unstable, neutrally stable, and stable conditions in traversing the Mach number range. The model oscillated in yaw from $M = 0.75$ to $M = 1.3$ where the trim attitude of the model was changed by the horizontal-tail motion and the model became dynamically stable. The data obtained from the model oscillations in yaw at the power-off conditions are presented in figures 13 to 16.

The measured period as a function of Mach number, presented in figure 13, shows an abrupt shift at $M = 0.96$. This change in period is more evident and distinctly present on a plot of period against flight time.

Static.- The static-directional-stability derivative $C_{n_\beta}{}^*$, obtained from the measured period, is shown in figure 14 as a function of Mach number. This $C_{n_\beta}{}^*$ curve indicates that a rearward shift of the lateral aerodynamic center occurs in going from subsonic to supersonic Mach numbers. Also indicated by the $C_{n_\beta}{}^*$ curve is a stability increase between $M = 1.0$ and $M = 1.15$; this increase is in a region which corresponds with that in which an increase in lift-curve slope for surfaces normally occurs. The C_{n_β} for the wing-fuselage combination, obtained from reference 10 for zero α, is shown in figure 14. The abrupt change in period and reflected change in $C_{n_\beta}{}^*$ which occurred at $M = 0.96$ corresponds to a changing lateral trim at the same Mach number.

A computation was made to determine the difference in $C_{n_\beta}{}^*$ obtained from a one-degree-of-freedom analysis and a reduction utilizing estimated derivatives by the three-degree-of-freedom assumption. The results indicate that $C_{n_\beta}{}^*$ is approximately 8.4 percent lower than C_{n_β}. References 11, 12, and 13 were used for estimating the derivatives and for computing the lateral motions.

Dynamic.- For the power-off conditions the lateral dynamic stability as a function of Mach number, given in figure 15, shows a region of neutral dynamic stability from $M = 0.75$ to $M = 0.88$, a region of dynamic stability from $M = 0.88$ to $M = 1.0$, and a region of dynamic instability from $M = 1.0$ to $M = 1.3$. Between $M = 1.3$ and $M = 1.5$, the model was trimmed to a higher angle of attack and was apparently dynamically stable.

For the power-on conditions and the model trim as shown in figure 5, no dynamic instability was apparent as the model traversed the Mach number range in accelerated flight.

Apparently two factors were of primary influence in the dynamic stability for the power-on conditions. The inclination of the principal axis was favorably changed by the additional mass of the rocket grain. The power-on trim attitude of the model was more positive below $M = 0.90$. Other factors believed to be minor are jet effects, small center-of-gravity change, effect of angle of attack on the derivatives, and so forth. A plot of η as a function of Mach number for the power-on and power-off conditions is shown in figure 16.

Lateral trim.- The trimmed side-force coefficient of the model is shown in figure 17. A significant factor of the lateral trim characteristics is that a change in lateral trim occurred at $M = 1.33$ when the inclination of the horizontal tail was changed. This trim change, which corresponds to a sideslip angle of approximately $\frac{1}{4}^\circ$, is not large in magnitude but introduced a transient lateral disturbance for rapid motions of the horizontal tail. Another change in C_Y trim occurs between $M = 0.88$ and $M = 0.98$. This transonic lateral trim change is estimated to be of the order of 0.4° sideslip.

Coupled Motion

Figure 18 presents a typical time history of the model flight for the low lift attitude, power-off condition. The sustained motion in the transverse direction can be explained by a dynamic instability for the low lift attitude. The motion in the normal direction as shown by the normal accelerometer and the angle-of-attack measurements is of the order of $\frac{1}{2}^\circ$ sustained angle-of-attack disturbance.

In order to determine the cause of the disturbance in the normal plane, the angle-of-attack motion was broken down into its two harmonic components. Figure 19 shows the experimental data points taken from the flight time history at a Mach number of 0.92. The two sinusoidal components, curves A and B, can be added to give the compounded motion which agrees very well with the experimental data. Curve A has the same

frequency as the lateral motion but there is a phase shift between this motion and the motion indicated by the transverse accelerometer. Curve B has a frequency twice that of the lateral motion and is also shifted by a phase angle.

The occurrence of motions in the normal plane that have frequencies twice that of the lateral motion can be satisfactorily explained by either the derivative C_{m_β} or by terms present in the equations of motion before linearization, such as the $p\dot{\psi}$ term in the equation for pitching motion. However, the frequency of the motion labeled curve A is different from the natural pitch frequency of the model (P = 0.31). The time history shows the horizontal tail to be oscillating, but only within 2 percent of the full-scale range of 8°. The correspondance of one pitch-plane frequency with the natural frequency in yaw remains unexplained and what, if any, part the elastic (spring and mass) control system plays in causing the oscillation is unknown.

CONCLUSIONS

A large-scale rocket-propelled model was tested in free flight at Mach numbers up to 1.5. The model which represented a possible low-drag airplane configuration had a 3-percent-thick, 60° triangular wing and a geometrically similar horizontal tail located on top of a sweptback vertical stabilizer. The horizontal tail was located approximately at 50 percent mean aerodynamic chord above the wing chord plane and had a tail length of 125 percent mean aerodynamic chord. From analysis of the flight test data and comparison with data from similar configurations, the following conclusions are presented:

1. No severe penalty in zero-lift drag was experienced because of the addition of a single vertical and horizontal tail to a low drag configuration.

2. The trimmed induced drag parameter of 0.51 obtained from the present test at a Mach number of 1.32 and values of lift coefficient up to 0.13 was high in comparison with the untrimmed values obtained from tests of similar configurations with and without tails but compared favorably with estimated trimmed values.

3. The trimmed drag and lift coefficients which resulted from a tail deflection of -8° at a Mach number of 1.4 were 0.0282 and 0.125, respectively.

4. The forcing of longitudinal motions by lateral oscillations can be a factor in causing low amplitude oscillations in the longitudinal plane.

Langley Aeronautical Laboratory,
National Advisory Committee for Aeronautics,
Langley Field, Va., July 2, 1954.

REFERENCES

1. Morrow, John D., and Nelson, Robert L.: Large-Scale Flight Measurements of Zero-Lift Drag of 10 Wing-Body Configurations at Mach Numbers From 0.8 to 1.6. NACA RM L52D18a, 1953.

2. Wallskog, Harvey A., and Morrow, John D.: Large-Scale Flight Measurements of Zero-Lift Drag and Low-Lift Longitudinal Characteristics of a Diamond-Wing—Body Combination at Mach Numbers From 0.725 to 1.54. NACA RM L53C17, 1953.

3. Mitchell, Jesse L., and Peck, Robert F.: An NACA Vane-Type Angle-of-Attack Indicator for Use at Subsonic and Supersonic Speeds. NACA RM L9F28a, 1949.

4. Gillis, Clarence L., Peck, Robert F., and Vitale, A. James: Preliminary Results From a Free-Flight Investigation at Transonic and Supersonic Speeds of the Longitudinal Stability and Control Characteristics of an Airplane Configuration With a Thin Straight Wing of Aspect Ratio 3. NACA RM L9K25a, 1950.

5. Bishop, Robert C., and Lomax, Harvard: A Simplified Method for Determining From Flight Data the Rate of Change of Yawing-Moment Coefficient With Sideslip. NACA TN 1076, 1946.

6. Den Hartog, J. P.: Mechanical Vibrations Second ed., McGraw-Hill Book Co., Inc., 1940, pp. 26-29.

7. Mitcham, Grady L., Crabill, Norman L., and Stevens, Joseph E.: Flight Determination of the Drag and Longitudinal Stability and Control Characteristics of a Rocket-Powered Model of a 60° Delta-Wing Airplane From Mach Numbers of 0.75 to 1.70. NACA RM L51I04, 1951.

8. Kelly, Thomas C.: Transonic Wind-Tunnel Investigation of the Aerodynamic Characteristics of a 60° Triangular Wing in Combination With a Systematic Series of Three Bodies. NACA RM L52L22a, 1953.

9. Peck, Robert F., and Mitchell, Jesse L.: Rocket-Model Investigation of Longitudinal Stability and Drag Characteristics of an Airplane Configuration Having a 60° Delta Wing and a High Unswept Horizontal Tail. NACA RM L52K04a, 1953.

10. Wiggins, James W.: Wind-Tunnel Investigation at High Subsonic Speeds of the Static Longitudinal and Static Lateral Stability Characteristics of a Wing-Fuselage Combination Having a Triangular Wing of Aspect Ratio 2.31 and an NACA 65A003 Airfoil. NACA RM L53G09a, 1953.

11. Campbell, John P., and McKinney, Marion O.: Summary of Methods for Calculating Dynamic Lateral Stability and Response and for Estimating Lateral Stability Derivatives. NACA Rep. 1098, 1952. (Supersedes NACA TN 2409.)

12. Ribner, Herbert S., and Malvestuto, Frank S., Jr.: Stability Derivatives of Triangular Wings at Supersonic Speeds. NACA Rep. 908, 1948. (Supersedes NACA TN 1572.)

13. Allen, H. Julian, and Perkins, Edward W.: Characteristics of Flow Over Inclined Bodies of Revolution. NACA RM A50L07, 1951.

TABLE I

PHYSICAL CHARACTERISTICS OF THE MODEL

Geometric

Wing:	
Area (included), sq ft	15.9
Span, ft	5.75
Aspect ratio	2.31
Mean aerodynamic chord, ft	3.50
Sweepback of leading edge, deg	60
Dihedral	0
Taper ratio	0
Airfoil section	NACA 65A003
Vertical tail:	
Area (included), sq ft	4.65
Height (from center line), ft	1.67
Aspect ratio	0.60
Sweepback of leading edge, deg	66.7
Taper ratio	0.28
Horizontal tail:	
Area, sq ft	1.59
Span, ft	1.92
Aspect ratio	2.31
Sweepback of leading edge, deg	60
Taper ratio	0
Airfoil section	NACA 65A003

Mass and Inertia

	Fully loaded	Grain expended
Moment of inertia:		
About X-axis, slug-ft^2	5.5	5.37
About Y-axis, slug-ft^2	83.9	68.2
About Z-axis, slug-ft^2	83.7	68
Principal axis inclination, deg	1.46	1.82
Weight, lb	431.0	333.6
Center of gravity, percent $\bar{c}$	21.7	23.6

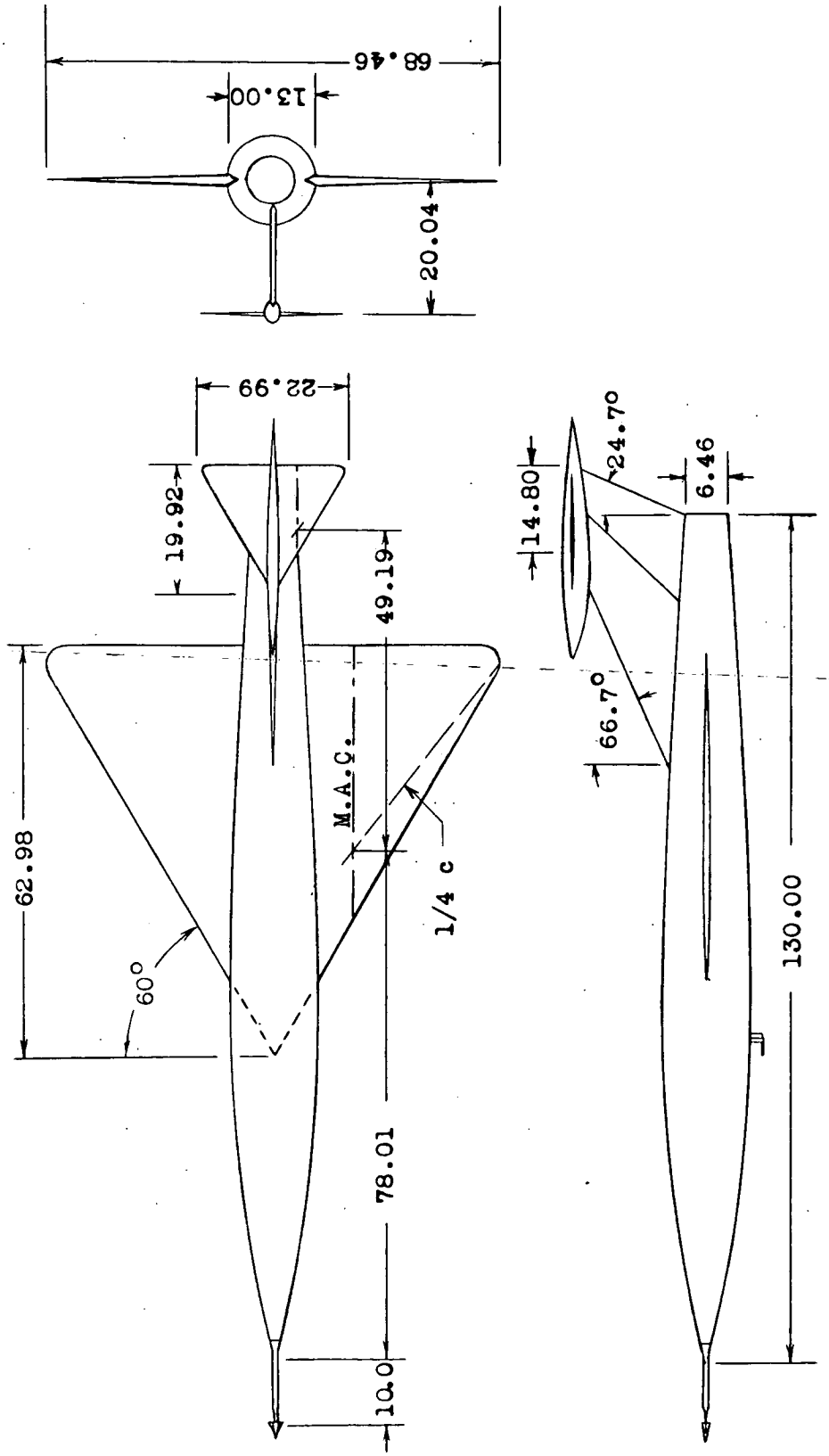

(a) Three-view drawing. All dimensions are in inches.

Figure 1.- Geometric characteristics of model.

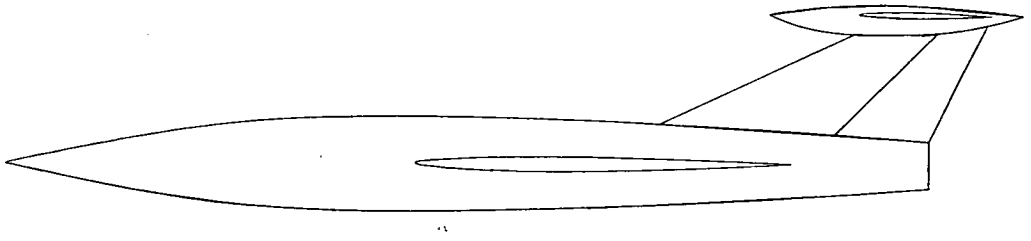

Model

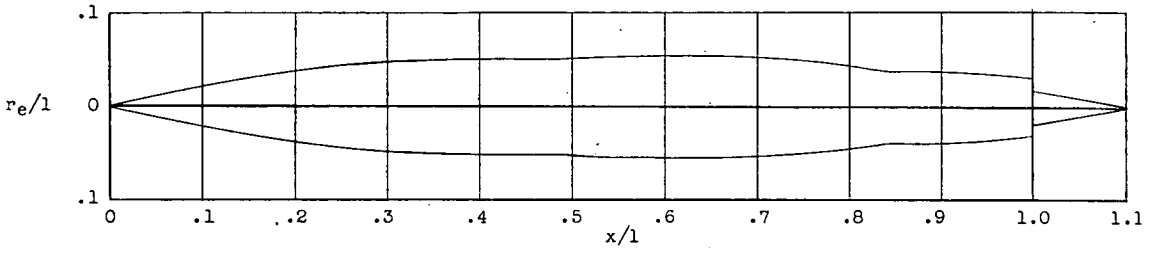

Equivalent body

l = 130 in.

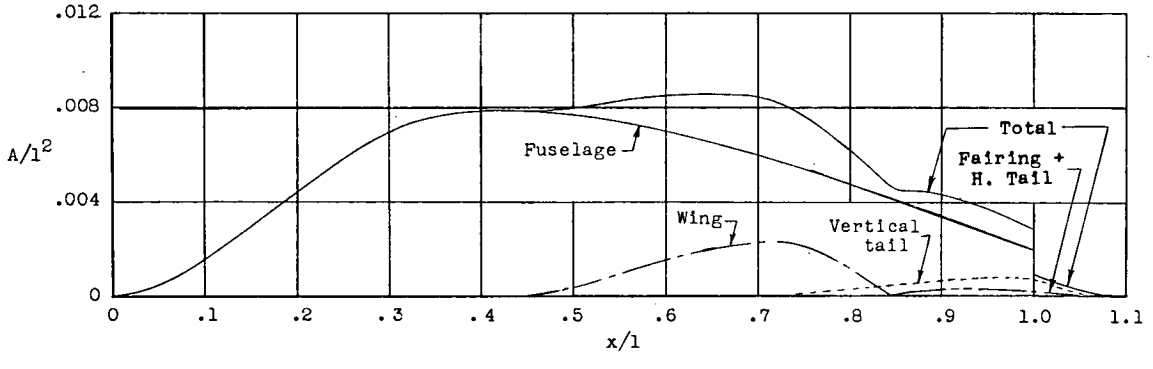

Area distribution

(b) Area distribution and equivalent body characteristics.

Figure 1.- Concluded.

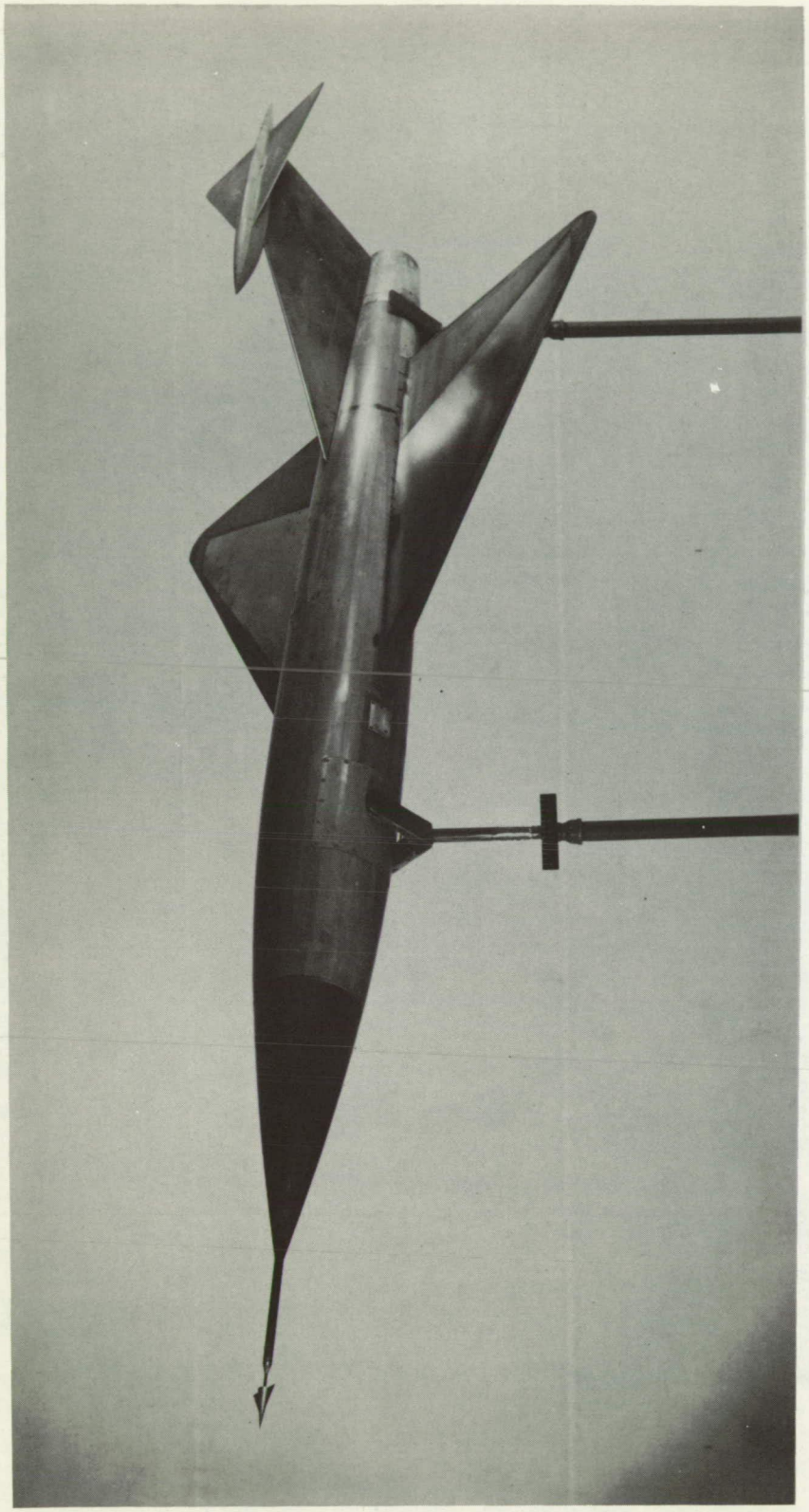

L-77104.1

(a) Three-quarter oblique view.

Figure 2.- Photographs of model.

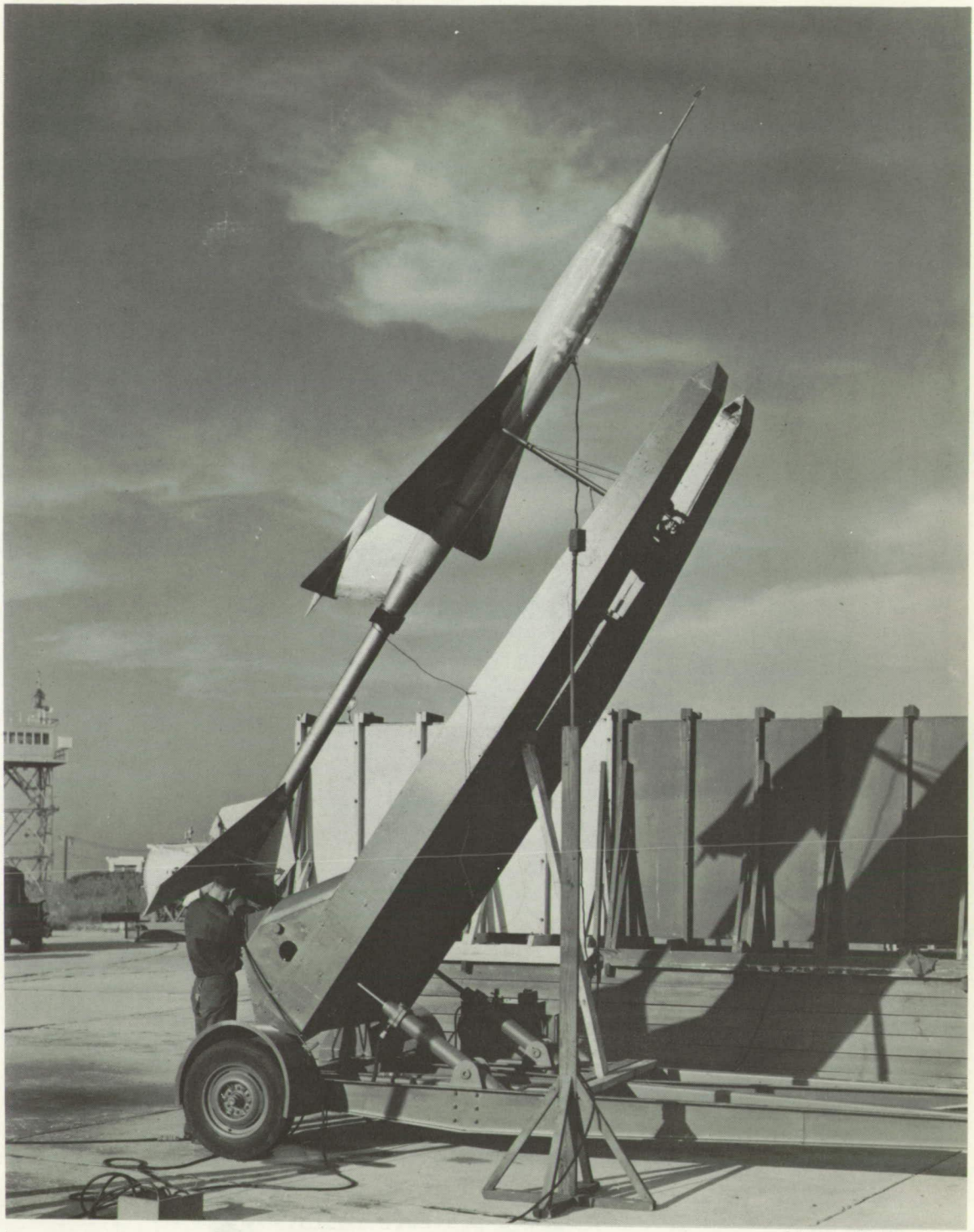

(b) Model on launcher. L-77513

Figure 2.- Concluded.

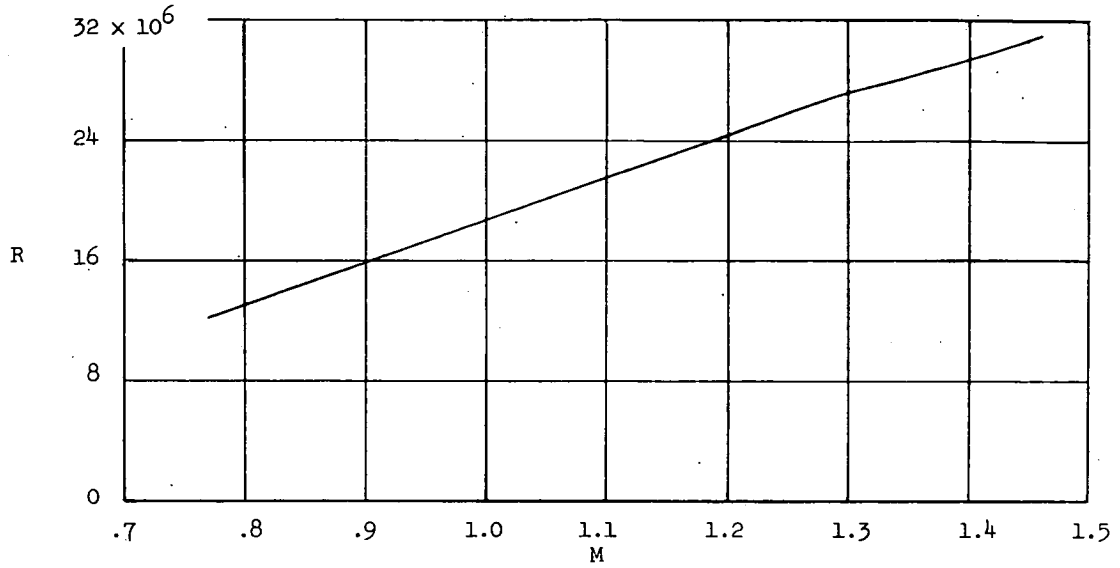

(a) Reynolds number.

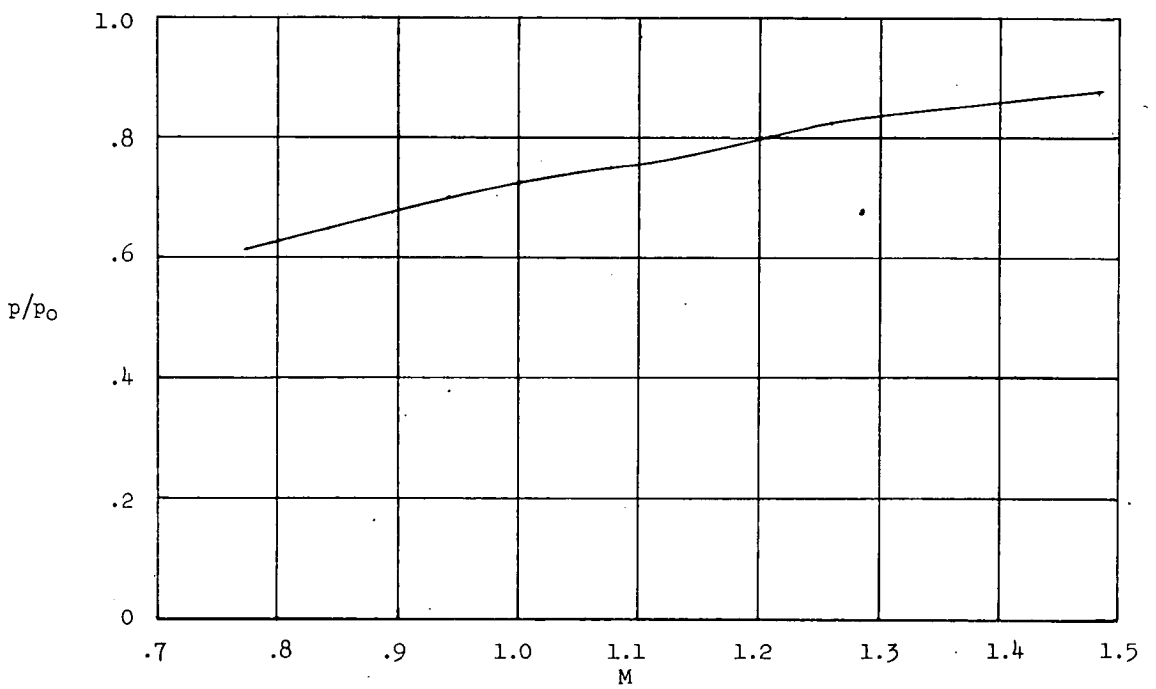

(b) Static-pressure ratio.

Figure 3.- Test conditions.

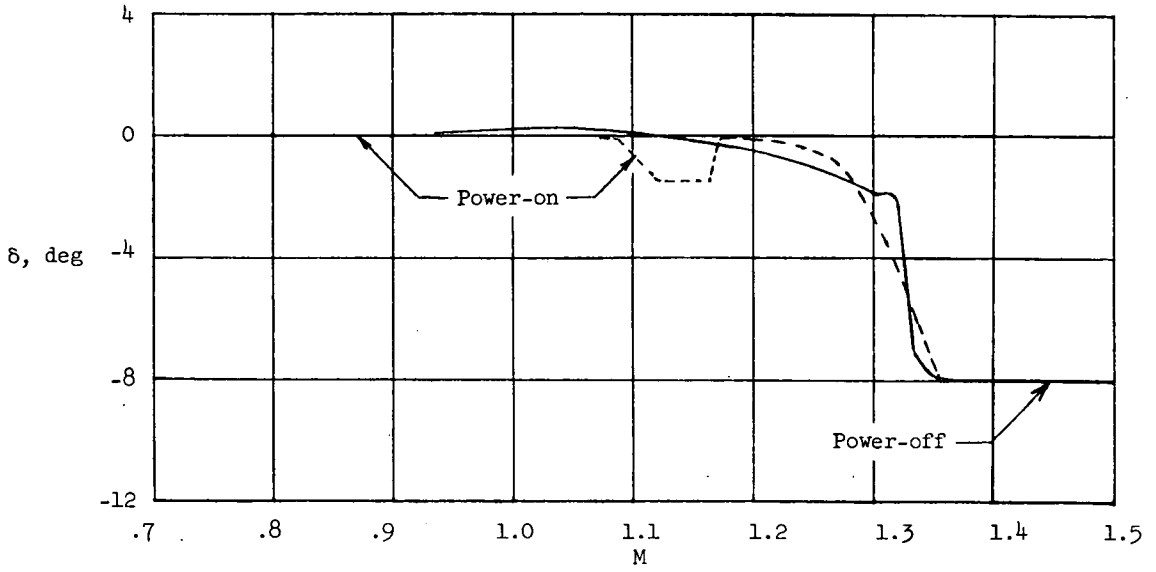

Figure 4.- Horizontal-tail position.

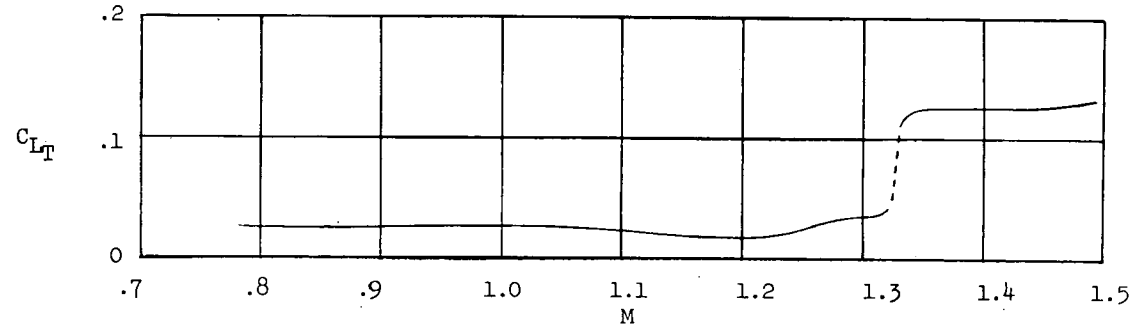

(a) Trim lift coefficient.

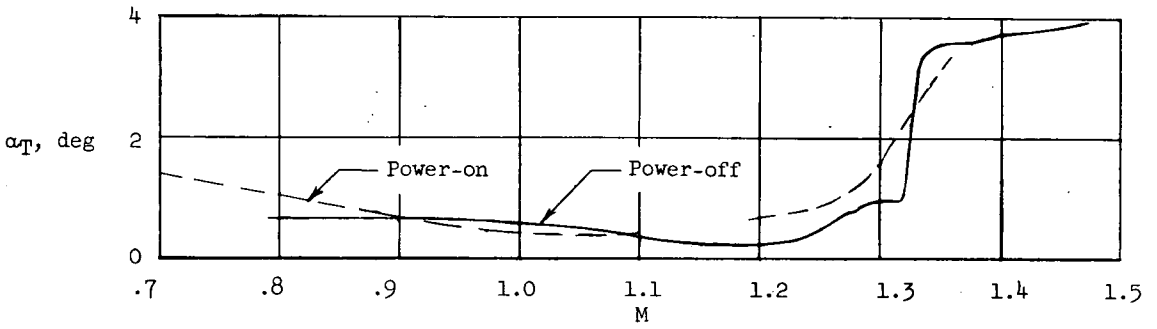

(b) Trim angle of attack.

Figure 5.- Model trim characteristics.

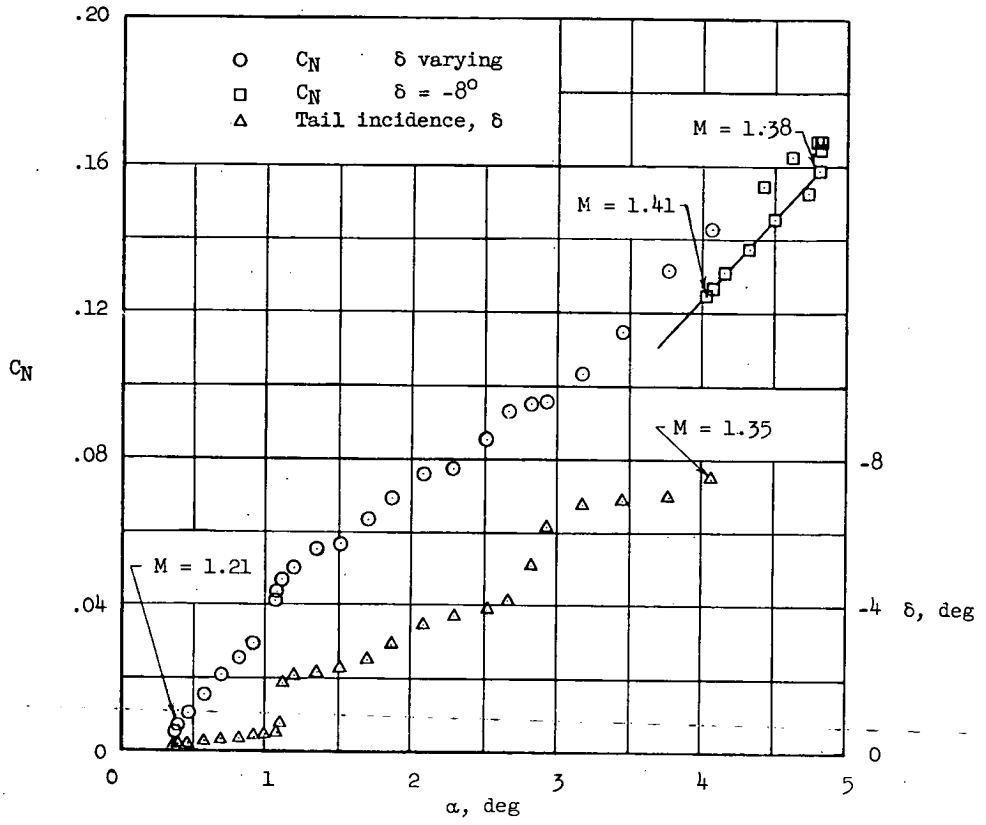

(a) Power on.

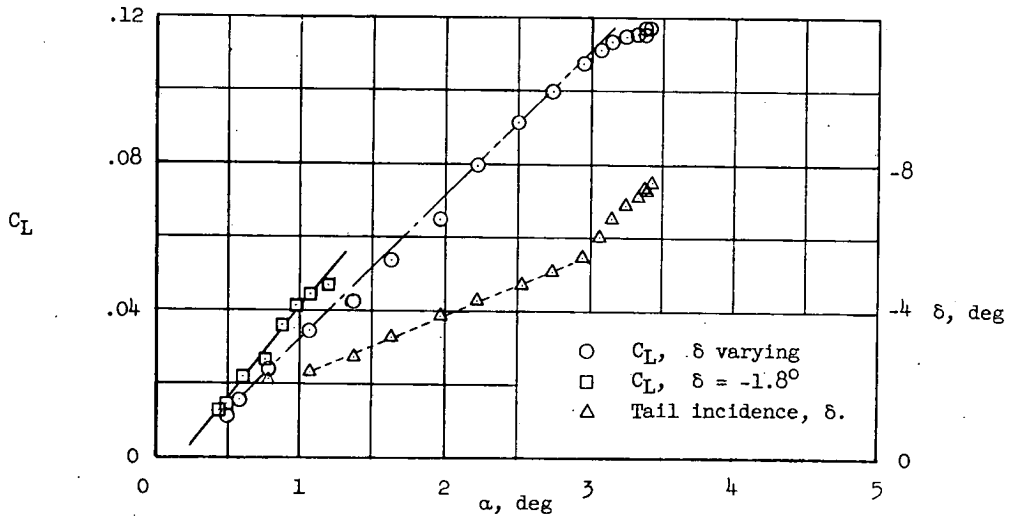

(b) Power off. M = 1.32.

Figure 6.- Variation of lift, normal force, and tail incidence with angle of attack.

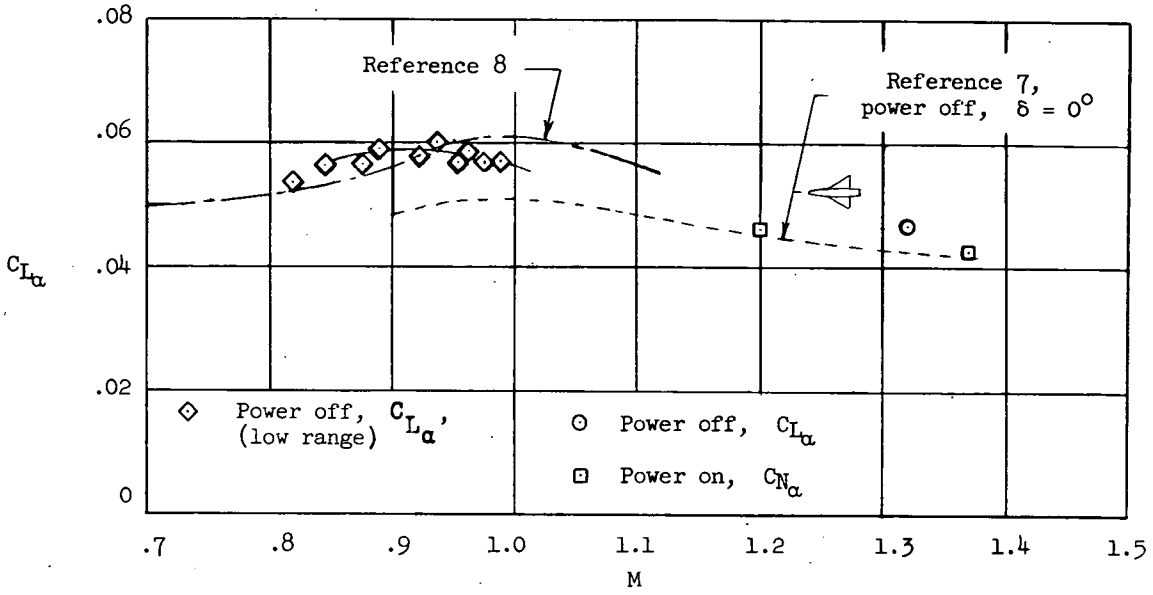

Figure 7.- Lift-curve slopes.

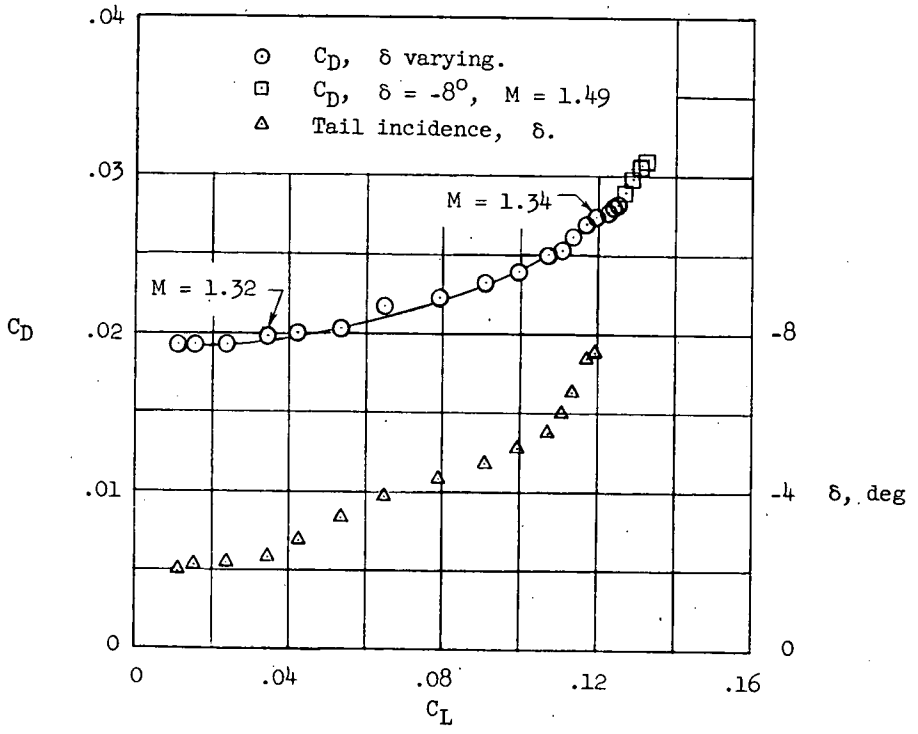

Figure 8.- Variation of drag with lift.

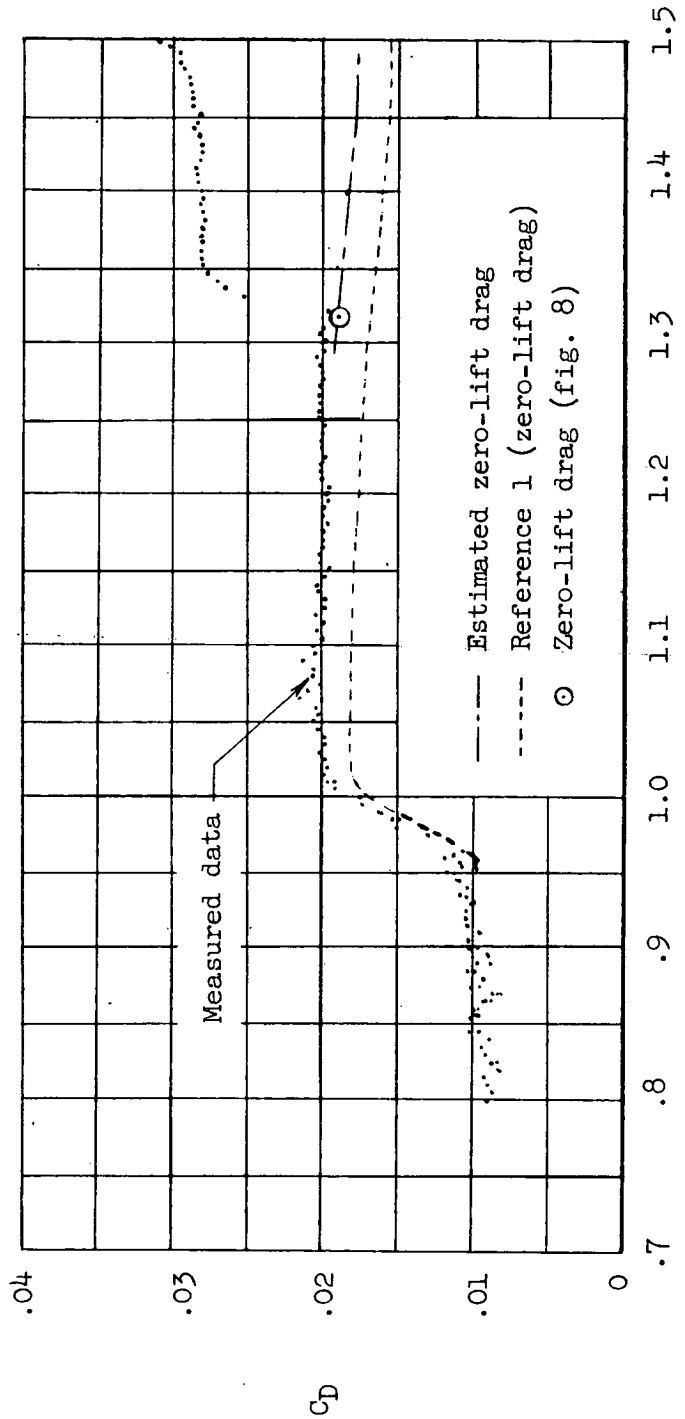

Figure 9.- Measured drag coefficients and estimated zero-lift drag.

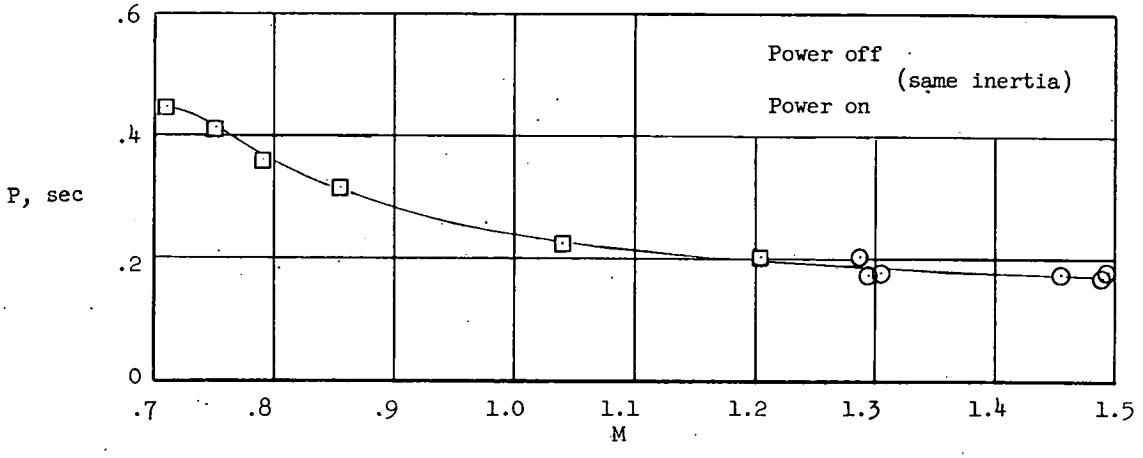

Figure 10.- Period of normal oscillation.

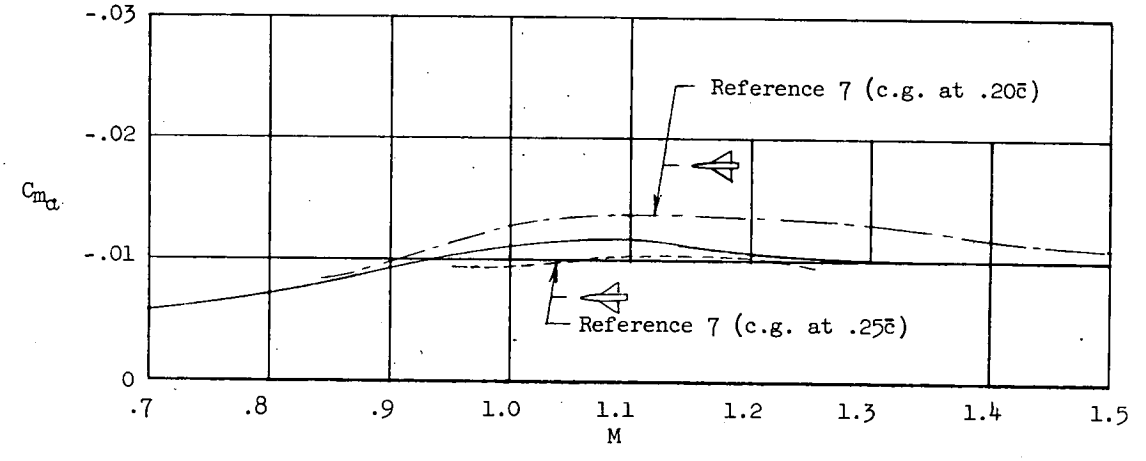

Figure 11.- Static longitudinal stability.

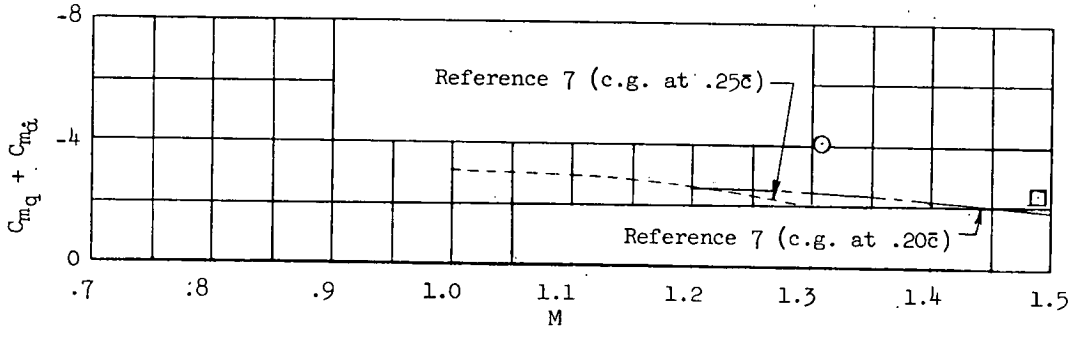

Figure 12.- Dynamic longitudinal stability.

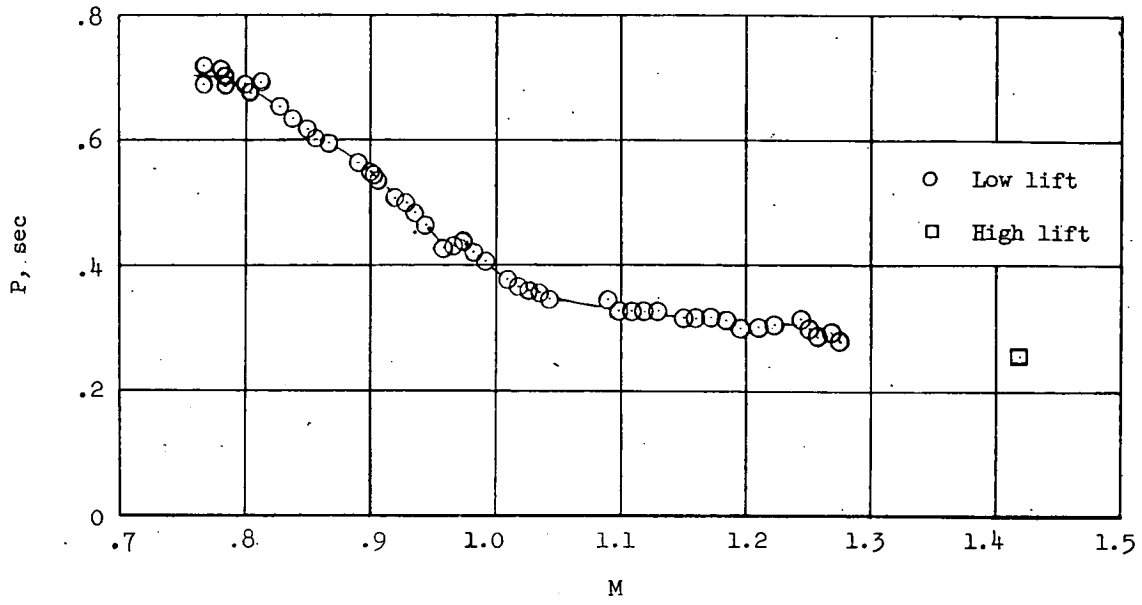

Figure 13.- Period of transverse oscillation. Power off.

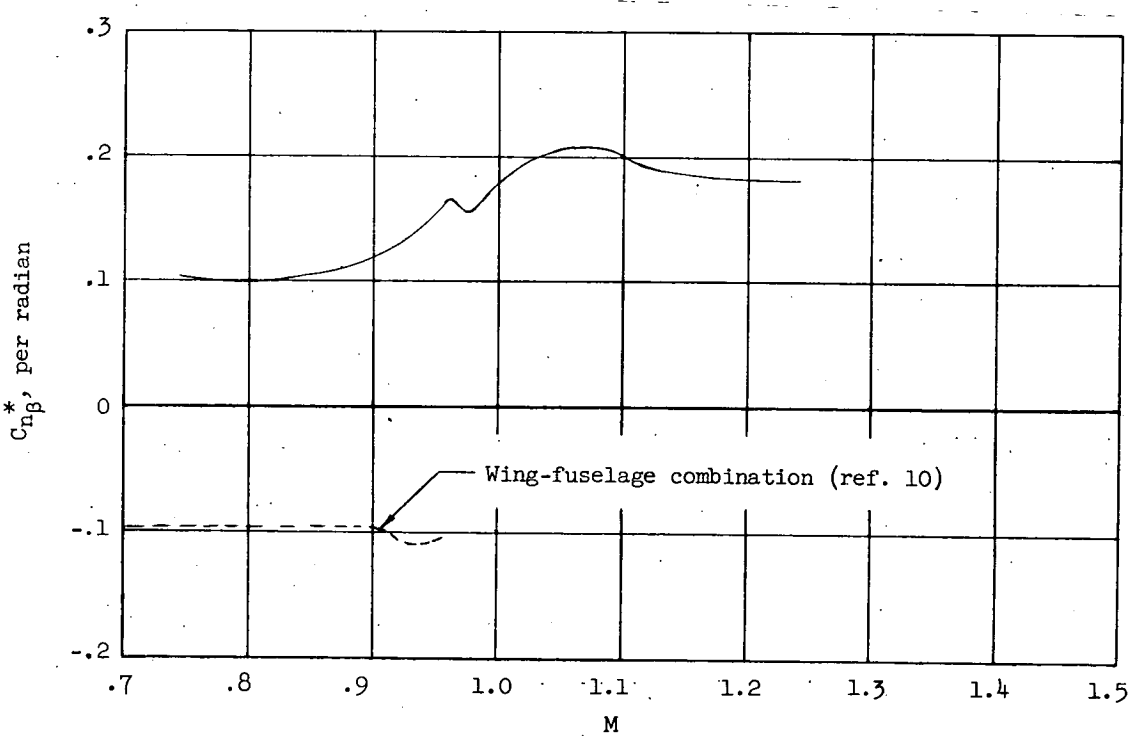

Figure 14.- Lateral static stability. Power off.

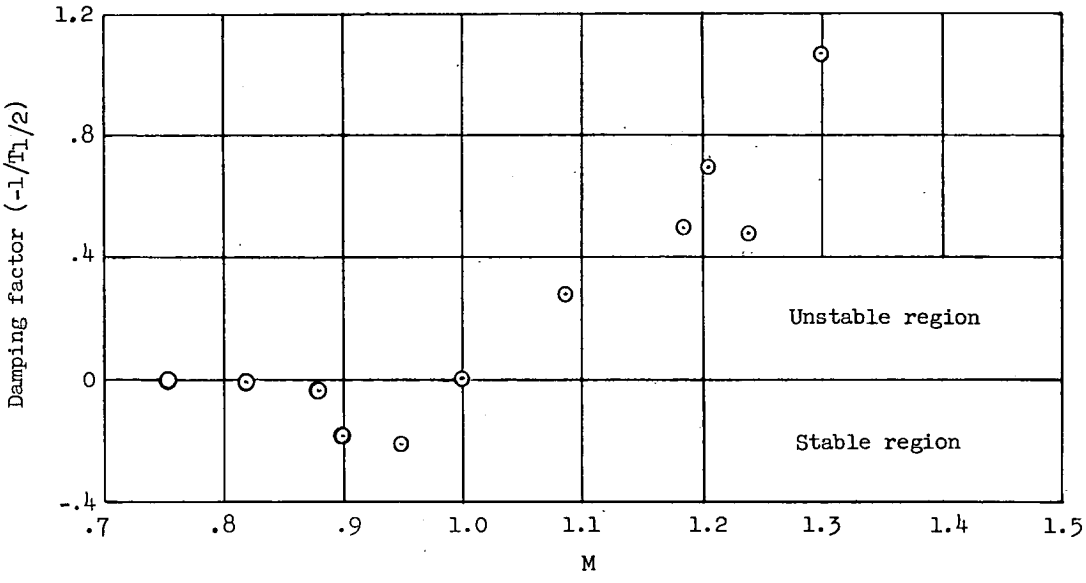

Figure 15.- Lateral dynamic stability. Power off.

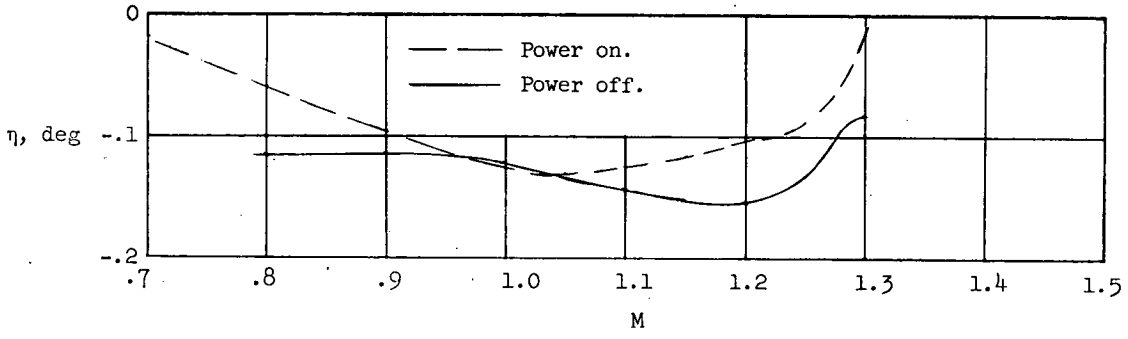

Figure 16.- Principal axis attitude.

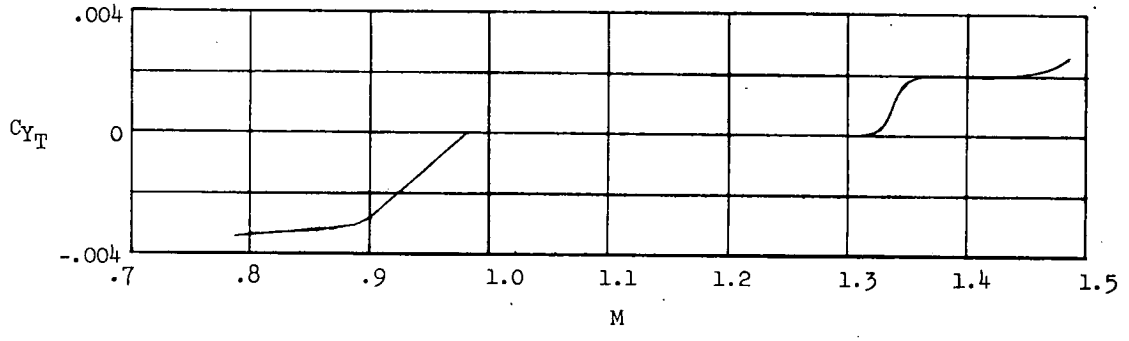

Figure 17.- Lateral trim characteristics. Power off.

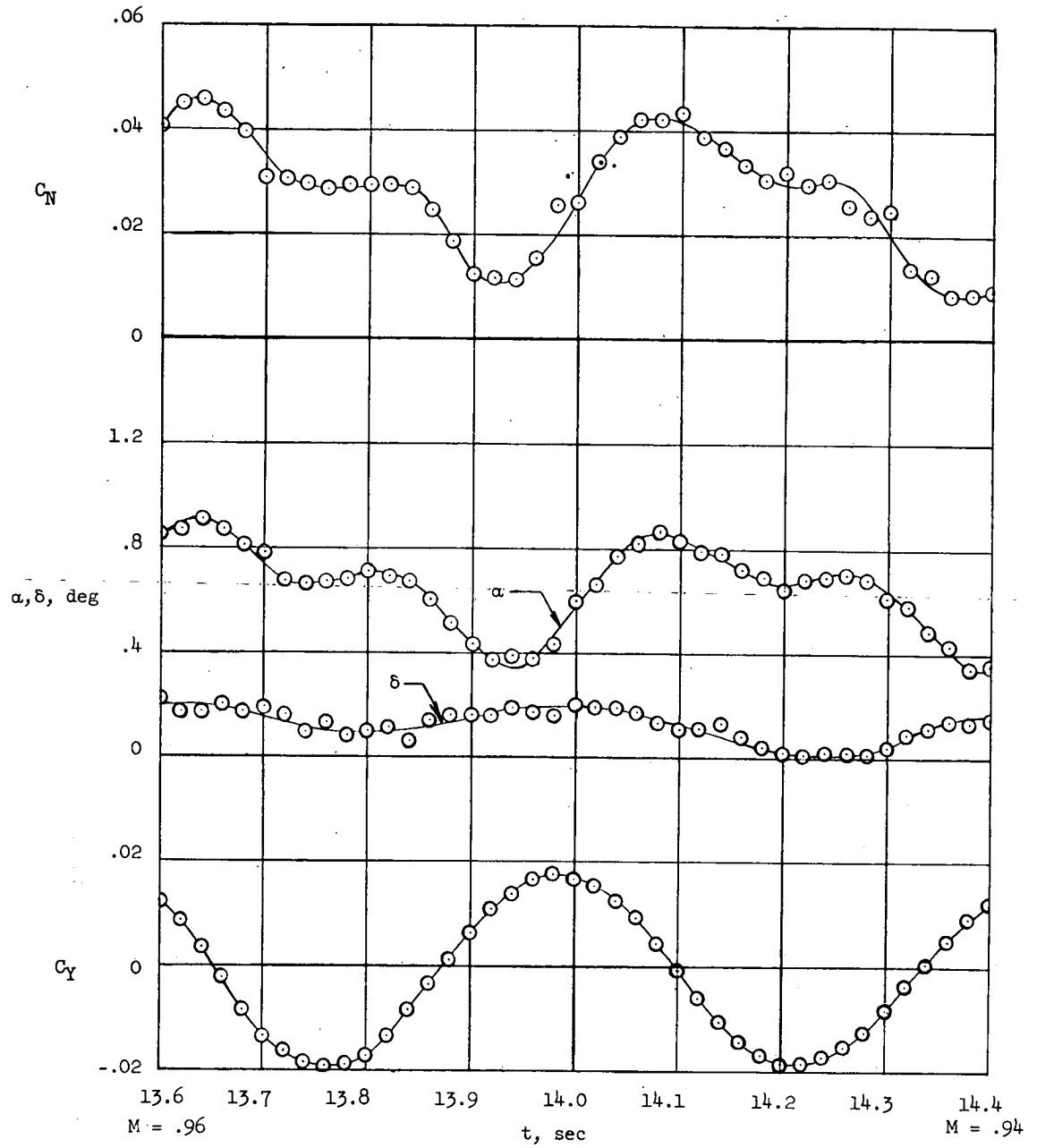

Figure 18.- Typical time history of motion at transonic speeds.

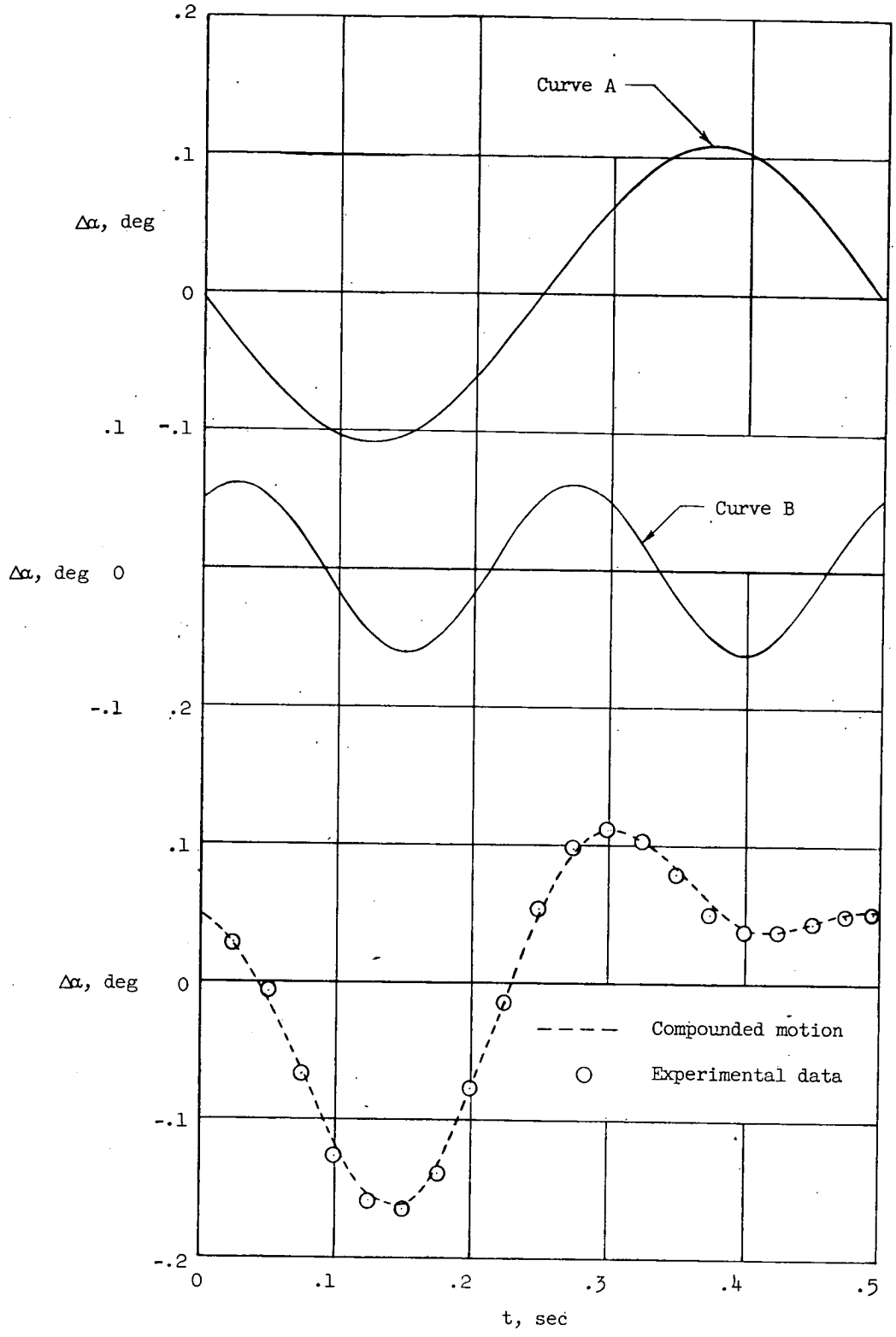

Figure 19.- Harmonic analysis of longitudinal motion.

NACA-Langley - 8-30-54 - 350